Progress in Physics of Applied Materials 5 (2025), 75 – 84

Semnan University

Progress in Physics of Applied Materials

journal homepage: https://ppam.semnan.ac.ir/

Comparative Study of Cu and Fe-Doped ZnO Nanoparticles: Synthesis, Characterization, and Multifaceted Bioactivities

Masome Naseri Tekyeh [a], Dariush Mehrparvar [a], Rostam Moradian [b]*, Shahriar Mahdavi [c], Maryam Rahimi [d], Mohammad Shahpouri [d]

[a] *Department of Physics, Faculty of Science, Malayer University, Malayer, Iran*

[b] *Department of Physics, Faculty of Science, Razi University, Kermanshah, Iran*

[b] *Department of Soil Science, Faculty of Agriculture, Malayer University, Malayer, Iran*

[b] *Department of Biology, Faculty of Science, Malayer University, Malayer, Iran*

ARTICLE INFO

Article history:
Received: 7 January 2025
Revised: 28 January 2025
Accepted: 11 February 2025

Keywords:
ZnO NPs;
Sol-gel Method;
Anticancer;
Antibacterial;
Antioxidant.

ABSTRACT

Metal oxide nanoparticles display significant roles in antimicrobial and anticancer activities. In the present study, Cu, and Fe-doped ZnO nanoparticles have been synthesized and investigated for their antioxidant, antibacterial, and anticancer properties. The above-mentioned nanoparticles have been synthesized by the low-cost and simple sol-gel method. The 2,2-Diphenyl-1-picrylhydrazyl (DPPH) assay was conducted to assess the antioxidant activity. The antibacterial activity of NPs was tested against E. coli and S. aureus bacteria according to the broth microdilution method in Mueller Hinton Broth. The anticancer potency on cancerous AsPC-1 cell lines was examined. The structural and morphology of samples confirm that all NPs formed with different crystallite sizes in the hexagonal wurtzite system. The DPPH assay showed the $Zn_{1-x}Cu_xO$ to have more antioxidant properties than other samples. We observed that the S. aureus bacterium is more sensitive to NPs than the E. coli bacterium. The strongest and weakest substances used for these bacteria are $Zn_{1-x}Cu_xO$ and $Zn_{1-x}Fe_xO$ NPs, respectively. Our anticancer results showed that the loaded drug on the NPs surfaces has more anticancer properties than pure drugs. ZnO and $Zn_{1-x}Fe_xO$ NPs possess similar anticancer properties approximately, while sunitinib@$Zn_{1-x}Cu_xO$ eliminates 92% of cancer cells at 200 µg/ml concentration. We observed that ZnO, $Zn_{1-x}Fe_xO$, and $Zn_{1-x}Cu_xO$ NPs have antioxidant, antibacterial, and anticancer properties. Adding copper dopant to ZnO NP significantly increases its anticancer property.

1. Introduction

Currently, various cancers have been the leading cause of human death with metastasis and secondary infection treatments of cancers have general methods like surgery [1], chemotherapy [2], radiotherapy, and immunology [3]. Therefore, one should find a way to overcome the resistance of cancer cells to usual treatments with less harmful side effects. In cancer therapy like the analgesics used during and after surgery might have on long-term outcomes such as cancer recurrence [4]. In addition, chemotherapy has frequent toxic side effects such as hepatitis, cholestasis, and steatosis [5]. Likewise, radiotherapy damages the DNA in surrounding healthy tissue of cancer cells and causes accelerated aging [6]. Microbial contamination is a pressing issue in health care, being responsible for nearly 40% of the 50 million global deaths annually due to diseases caused by bacteria like Escherichia coli and Salmonella [7, 8]. Different therapeutic applications have been paved using various nanomaterials with recent developments in nanotechnology [9], so they are of considerable interest. Multi-functional metals and metal oxide NPs have significant applications in antimicrobial activities, biomedicine, pharmaceutics, food industry and healthcare

* Corresponding author. Tel.: +98-918-1324809
E-mail address: **moradian.rostam@gmail.com**

Cite this article as:
Naseri Tekyeh M., Mehrparvar D., Moradian R., Mahdavi Sh., Rahimi M. and Shahpouri M., 2025. Comparative Study of Cu and Fe-Doped ZnO Nanoparticles: Synthesis, Characterization, and Multifaceted Bioactivities. *Progress in Physics of Applied Materials*, *5*(1), pp.75-84. DOI: **10.22075/PPAM.2025.36408.1127**

[10-12]. Metal oxide NPs like: TiO_2 [13], ZnO [14], CuO [15], SiO_2 [16], SnO_2 [17], and MgO [18] exhibit interesting antibacterial properties and anticancer potential [19-22]. Among these, ZnO has been particularly noted for its anticancer and antibacterial activity [23, 24]. Also, it has been indicated by several researchers that ZnO nanostructures can be successfully used against various cancer cell lines [25-28], both gram-positive and gram-negative bacteria [29-32]. Zinc oxide is an affordable, non-toxic, and well-behaved metal oxide suitable for therapeutic applications compared to other metal oxides. Antioxidants contribute to enhancing the body's natural antioxidant defense mechanisms. They support the body's production of endogenous antioxidants and activate various enzymes involved in antioxidant pathways, such as superoxide dismutase, catalase, and glutathione peroxidase. These protective systems collaborate to maintain balance and prevent the organism from experiencing excessive oxidative stress [33].

We synthesized ZnO NPs with Fe and Cu dopants using a simple and affordable sol-gel method and investigated their antioxidant, antibacterial, and anticancer activity. Additionally, the anticancer drug (sunitinib) was loaded on the ZnO NPs and compared with the NP's anticancer properties which will provide novel opportunities in cancer nanotechnology.

The experimental research procedure is shown as a schematic in Fig. 1.

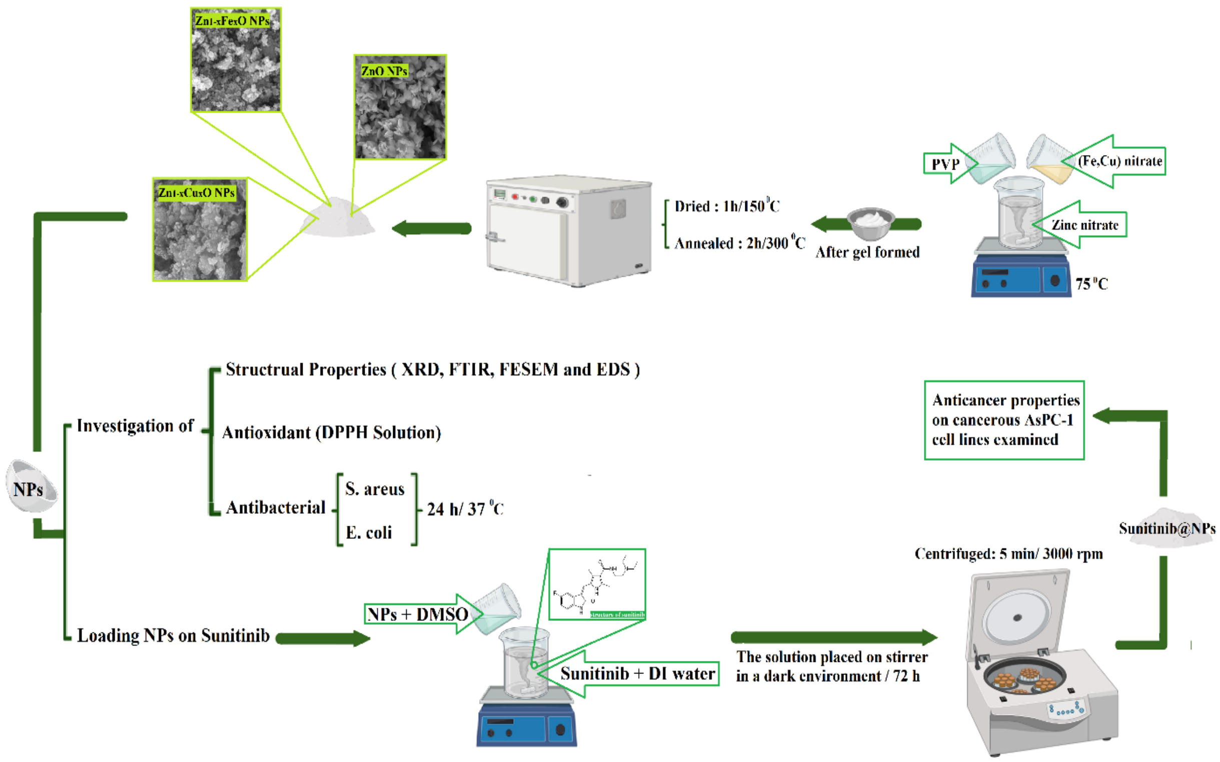

Fig. 1. Schematic of the experimental procedure

2. Materials and methods

2.1. Material

The chemicals used in this study were laboratory-grade and prepared by Merck, and chemical materials include Zinc nitrate hexahydrate ($Zn(NO_3)_2.6H_2O$), Iron (II) nitrate nonahydrate ($Fe(NO_3)_2$), Copper (II) nitrate trihydrate ($Cu(NO_3)_2.3H_2O$) and Polyvinylpyrrolidone (PVP) ($(C_6H_9NO)_n$. Deionized water, dimethyl sulfoxide (DMSO, C_2H_6OS), DPPH (2,2-diphenyl-1-picrylhydrazyl), and methanol (CH_3OH) were also used. For the antibacterial test, E. coli[1] (ATCC 25922, negative gram) and S. aureus[2] (ATCC 29213, positive gram) bacteria were purchased from IROST[3]. To test for anticancer, sunitinib 25 mg capsule and AsPC-1 cell line belonging to human pancreatic cancer were supplied from the Pasteur Institute of Iran.

2.2. Method

The following describes the synthesis method of pure and doped ZnO NPs.

Undoped ZnO NP Synthesis:

At first, 1 g of zinc nitrate hexahydrate (a source of zinc) is dissolved in 10 ml of methanol to prepare the precursor solution. The precursor solution is placed on the stirrer and stabilized at 70 °C. Then, 0.1 g of PVP is dissolved in 5 ml of distilled water which acts as a stabilizer or surfactant, helping to control the size and shape of the NPs. This solution is then added to the precursor solution. The mixture solution is heated to 75 °C to induce gel formation. This means the liquid solution thickens and forms a semi-

1 Escherichia coli

2 Staphylococcus aureus

3 Iran Scientific and Industrial Research Organization

solid gel. After that, the gel is dried at 150 °C for 1 hour to leave behind a dry powder. Finally, the powder is annealed at 300 °C for 2 hours. This step helps to crystallize the material, improving its structural properties [34].

Doped ZnO NPs Synthesis:

The target concentration of the dopants (Fe or Cu) in the ZnO nanostructure is 10 weight percent. Dopant sources were iron and copper using iron (II) nitrate and copper (II) nitrate, respectively. The iron or copper nitrate is dissolved in 10 ml of methanol to prepare the doping resources. This solution is then added to the initial zinc nitrate solution before gel formation. In the final step, the PVP solution added them. The rest of the process (gel formation, drying, annealing) is similar to the undoped ZnO preparation.

Load Sunitinib Capsules on NPs:

To load the sunitinib drug on the ZnO NPs, two 25 mg sunitinib capsules were dissolved in 5 ml deionized water and stirred until completely resolved as the primary solution. 0.2 g of NPs were poured into 5 ml of DMSO until completely dissolved in the solution. The NP solution was added to the primary solution and stirred in a dark environment for 72 h. After the reaction time, the final solution was centrifuged at 3000 rpm for 5 minutes.

Antioxidant Activity:

To assess the antioxidant activity of ZnO NPs, the DPPH assay was conducted following the methodology described by Miliauskas et al., with minor adjustments [35]. In this experiment, a 0.1 mM ethanolic DPPH solution (4 mL) was prepared, and 3 mL of the NP solution was added to the DPPH solution. The mixture was thoroughly vortexed to ensure proper mixing. After an incubation period, the solution's absorbance was measured at 517 nm using a UV-Vis spectrophotometer (Spectrum SP-UV500DB). The DPPH radical activity was determined using the following formula [36]:

$$\text{Antioxidant activity} = \frac{(z - x)}{z} \times 100\% \tag{1}$$

The absorbance value denoted as **z** represents the control parameter, while it is denoted as **x** for the sample.

Antibacterial Activity:

The antibacterial effectiveness of NPs was evaluated against two types of bacteria: the gram-negative Escherichia coli (E. coli, ATCC-25922) and the gram-positive Staphylococcus aureus (S. aureus, ATCC-25923). This assessment was carried out using the broth microdilution method in Mueller Hinton Broth (MHB), a widely used culture medium that supports the growth of these bacterial species and allows for precise determination of antimicrobial activity. The bacteria strains were cultured in trypticase Soy Broth (TSB) and incubated for 24 hours at 37°C. After incubation, the culture medium containing the grown bacteria was centrifuged at 5000 rpm for 20 minutes, the supernatant was discarded and the bacteria were washed twice with normal saline. Finally, the precipitated contents were dissolved with physiological serum and reached a concentration of 0.5 McFarland standard (1.5 x 10^8 CFU/ml) [37]. The bacterial suspension was used as inoculum in the antibacterial assays.

Serial dilutions of the NPs were prepared to achieve initial concentrations in TSB, resulting in final concentrations of 1024, 512, 256, 128, 64, 32, 16, 8, 4, and 2 mg/l on a plate. After adding 100 µl of bacterial inoculum to each suspension, it was incubated at 37 °C for 24 hours. After the incubation period, the microplates were read using an ELISA reader at a wavelength of 600 nm. The minimum lethal concentration of NPs for bacteria was also investigated [38]. At the end of the experiment, the percentage of inhibition of microbes in the presence of NPs was calculated using the following formula [39]:

$$\text{Inhibition rate} = \frac{(D_{\text{control}} - 0.5) - (D_{\text{treatment}} - 0.5)}{(D_{\text{treatment}} - 0.5)} \times 100\% \tag{2}$$

where D means colony diameter, the higher the inhibition rate value shows stronger the inhibitory effect.

Anticancer Activity:

We tested the anticancer activity of samples using the AsPC-1 cell line of human pancreatic cancer. The cell line was cultured in culture medium RPMI (BIO-IDEA; Iran) containing 10% FBS (Gibco; USA) and 1% antibiotic (BIO-IDEA; Iran). To evaluate cytotoxicity, we conducted a detailed assay using the 3-(4,5-dimethylthiazol-2-yl)-2,5-diphenyltetrazolium bromide (MTT) method, sourced from Sigma Aldrich. This assay measures cell viability based on the metabolic activity of living cells. After treatment, we quantitated the intensity of the resulting color, which correlates directly to the number of viable cells. This approach provides us with insight into the cytotoxic effects of the tested compounds, allowing for a thorough understanding of their potential impact on cellular health. At first, 3×10^3 cells per ml and ZnO NPs were seeded in each well of a 96-well plate. After 24 hours, 10 ml of MTT solution with 5 mg/ml concentration was added to the cell culture medium, and the plate was incubated for 3 hours. Then the cell supernatant was removed, and 80 µl of DMSO was added to each well. After 30 minutes, the contents of the wells were pipetted several times to flush out the sediment inside the cells. The optical density (OD) from the solution dye was assessed at 570 nm employing an ELISA reader. The cell viability rate (VR) an important measure used to assess the health and functionality of cells in various experimental contexts, was calculated by the following equation [40]:

$$\text{VR} = \frac{A}{A_0} \times 100\% \tag{3}$$

where A represents the absorbance of the cells treated with formulations and A_0 refers to the absorbance of the control group.

3. Structural Characterization

The crystal structure of the samples was characterized using X-ray diffraction (XRD) with a Philips instrument, Energy-dispersive X-ray spectroscopy (EDS) using a TESCAN VEGA 3, and Fourier transform infrared spectroscopy (FT-IR) with a Thermo AVATAR. The morphology of the NPs was investigated using field emission scanning electron microscopy (FESEM) with a TESCAN MIRA III.

4. Results and Discussion

The XRD patterns of nanostructures of ZnO, Zn1-xFexO, and Zn1-xCuxO are presented in Fig. 2, that the diffraction peaks observed in all samples correlate with the standard diffraction pattern for ZnO crystals JCPDS (01-072-0627), which features a hexagonal wurtzite-type structure [41]. Since there are no additional peaks beyond those of undoped ZnO in the diffraction patterns of Zn1-xFexO and Zn1-xCuxO, it can be concluded that the samples have a single-phase crystalline structure consistent with bulk ZnO. This indicates that some of the zinc sites in the ZnO nanostructures have been substituted with iron (Fe) and copper (Cu). The Miller indices for the planes corresponding to each peak are illustrated in Fig. 2.

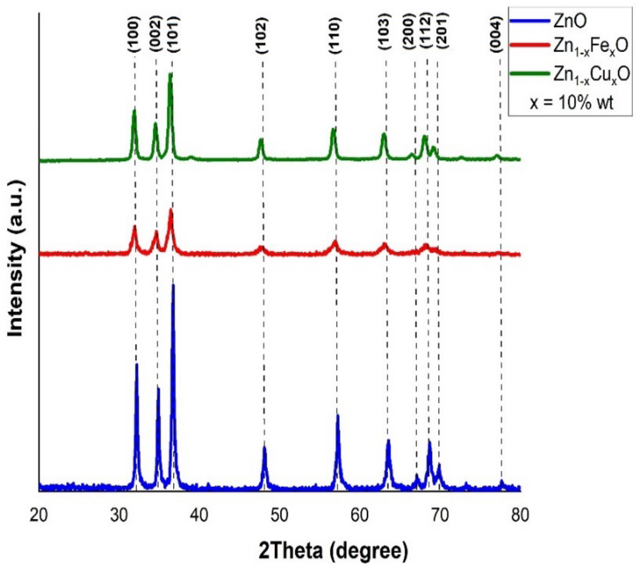

Fig. 2. XRD patterns of the ZnO, $Zn_{1-x}Fe_xO$, and $Zn_{1-x}Cu_xO$ NPs

By analyzing the peak widths obtained from the X-ray diffractogram, we can accurately estimate the average diameter of the nanocrystals. The average size of the nanocrystals was determined using the well-known formula of Scherrer equation [42]:

$$D=\frac{0.9\lambda}{\beta\cos\theta} \tag{4}$$

In this context, D, λ, β, and θ represent the crystal size, the wavelength of the X-ray source (0.154 nm), the broadening of the diffraction line at full-width half maximum, and the position of the diffraction peaks, respectively. The crystallite size is obtained by averaging over the size of all the peaks. They are given in Table 1.

Table 1. The crystallite size of NPs

Dopant source	D (nm)
Bare	31.98
Fe	32.09
Cu	58.82

The results presented in Table 1 indicate that the addition of Cu and Fe dopants leads to a slight variation in the crystallite size compared to the bare sample. This difference is likely due to a minor mismatch among the Zn, Fe, and Cu ions. The findings suggest that the Cu and Fe ions effectively replace the Zn ions in the samples without significantly altering the overall crystal structure [43], and the type of impurity causes a change in the crystallite size.

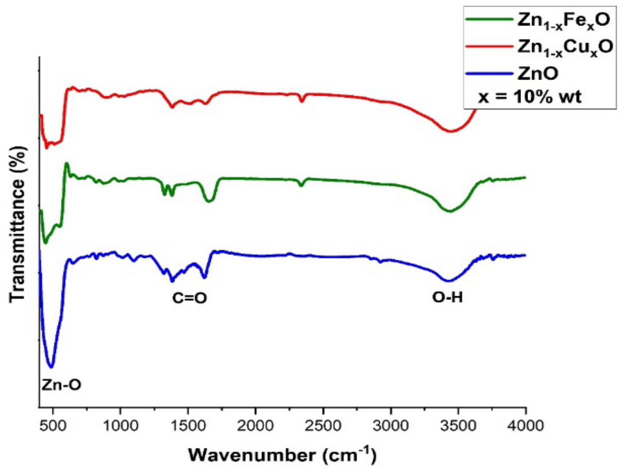

Fig. 3. FTIR spectra of ZnO prepared samples

FTIR spectra of the NPs were presented in Fig. 3, in the range of 400-4000 cm^{-1}. The peak observed between 450-500 cm^{-1} is attributed to the stretching modes of Zn-O [44]. The reduction in the intensity of the Zn-O peak is due to the substitution of impurities in the Zn position by adding impurities. The broad peak between 3200-3600 cm^{-1} is associated with the bands of bonded hydroxyl groups of the vibration of adsorbed water molecules [45]. In addition, two distinct peaks are observed at 1072 cm^{-1} and 1356 cm^{-1}, which are characteristic of the carboxyl group [45].

The NP morphologies were analyzed using the FESEM technique, as shown in Fig. 4. The results indicate that the formation of hexagonal ZnO varies with different dopant elements, and impurities have notably altered the morphology.

The energy dispersive X-ray spectroscopy (EDS) analysis of the NPs presented in Fig. 5 indicates that the ZnO NPs exhibit peaks corresponding only to 'Zn' and 'O'. In contrast, the doped ZnO NPs also display peaks for 'Fe' and 'Cu', confirming the incorporation of iron and copper ions into the ZnO lattice, is accompanied by a reduction in the percentage of zinc.

In Fig. 6, the scavenging percentages of DPPH were measured to assess the antioxidant activity. As we know, The DPPH assay is a relatively simple and widely used method for evaluating a substance's antioxidant capacity. DPPH is a stable free radical. In its radical form, it has a deep violet color and absorbs strongly at a specific wavelength (usually around 515-520 nm). This strong absorbance allows us to track changes in its concentration using a spectrophotometer. When an antioxidant molecule is added to the DPPH radical solution, the antioxidant donates either a hydrogen atom or an electron to the DPPH radical. This neutralizes the DPPH radical, converting it to its non-radical form (DPPH-H).

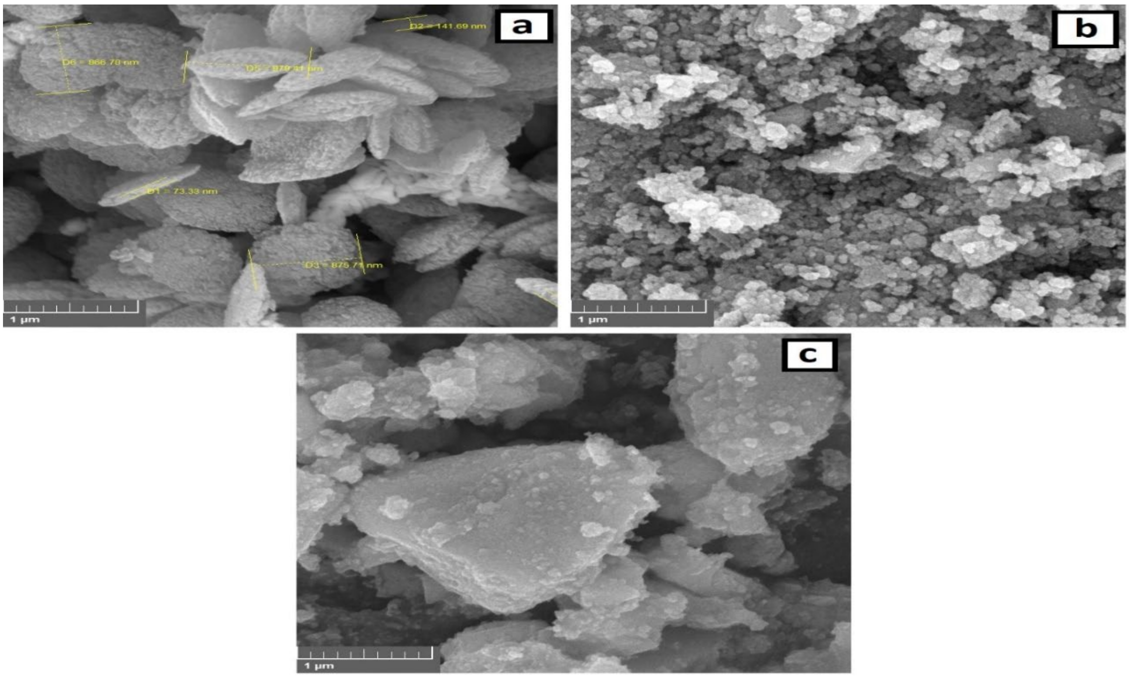

Fig. 4. FESEM images of (a) ZnO, (b) $Zn_{1-x}Fe_xO$ and (c) $Zn_{1-x}Cu_xO$ NPs

As the DPPH radical gets neutralized, the violet color of the solution fades. The extent of this color change is directly proportional to the antioxidant capacity of the tested substance. The more antioxidants present in the sample, the more DPPH radicals will be reduced, leading to a greater decrease in absorbance (and lighter color). This color change is measured using a spectrophotometer where DPPH absorbs most strongly [46, 47].

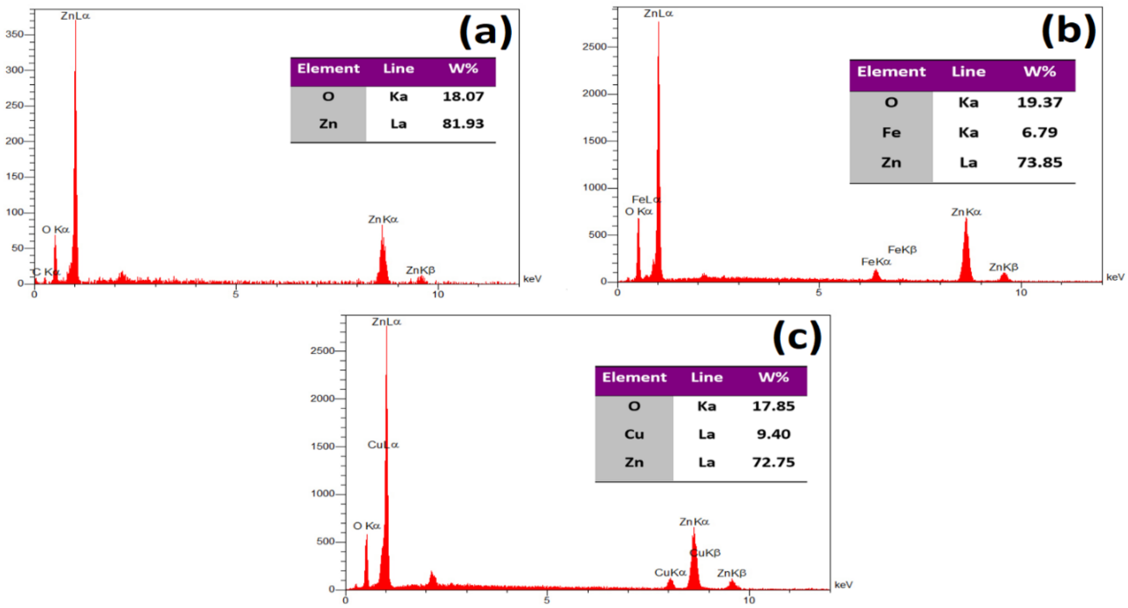

Fig. 5. EDS of the (a) ZnO, (b) $Zn_{1-X}Fe_XO$, and (c) $Zn_{1-X}Cu_XO$ NPs

The radical scavenging percentages for different samples were as follows: ZnO exhibited a scavenging percentage of 48.46 ± 2.23, $Zn_{1-x}Fe_xO$ showed 69.12 ± 4.34, $Zn_{1-x}Cu_xO$ demonstrated 88.98 ± 3.43, and EU80PEG20Gin10% displayed 73.16 ± 3%. Fig. 6, shows that adding impurity improved the antioxidant properties, and copper dopant was more suitable than iron.

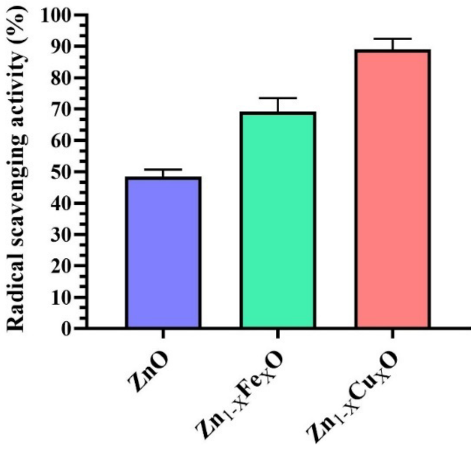

Fig. 6. Antioxidant properties of ZnO NPs

Fig. 7 shows the inhibition percentage of S. aureus and E. coli bacteria by NPs. Based on the results obtained from this experiment, $Zn_{1-x}Cu_xO$ NPs showed more powerful antibacterial effects than the other two NPs, and $Zn_{1-x}Fe_xO$ had the least inhibitory effect on both bacteria. Among the bacterial samples tested, S. aureus bacterium (gram-positive) was more sensitive to NPs (Fig. 7a), and E. coli (gram-negative) one showed more resistance to NPs (Fig. 7b). Both bacterial types are affected by reactive oxygen species (ROS) generated by NPs. However, S. aureus bacterium is more vulnerable to oxidative damage due to its simpler cell wall and fewer protective mechanisms compared to E. coli one. This increases the effectiveness of NPs in disrupting S. aureus bacterium and also Copper ions released from $Zn_{1-x}Cu_xO$ NPs contribute to the antibacterial effect, and S. aureus bacterium is generally more sensitive to copper due to less efficient regulation of copper uptake compared to E. coli bacterium. Although both bacteria can form biofilms, S. aureus bacterium typically has a more robust biofilm structure, which may make it more susceptible to NP penetration if the NPs are highly reactive. In contrast, E. coli bacterium has more efficient mechanisms for expelling NPs, which may contribute to its higher resistance. E. coli bacterium strains often possess more mechanisms for resisting antimicrobial agents, such as efflux pumps, which might reduce the effectiveness of NPs against it compared to S. aureus one.

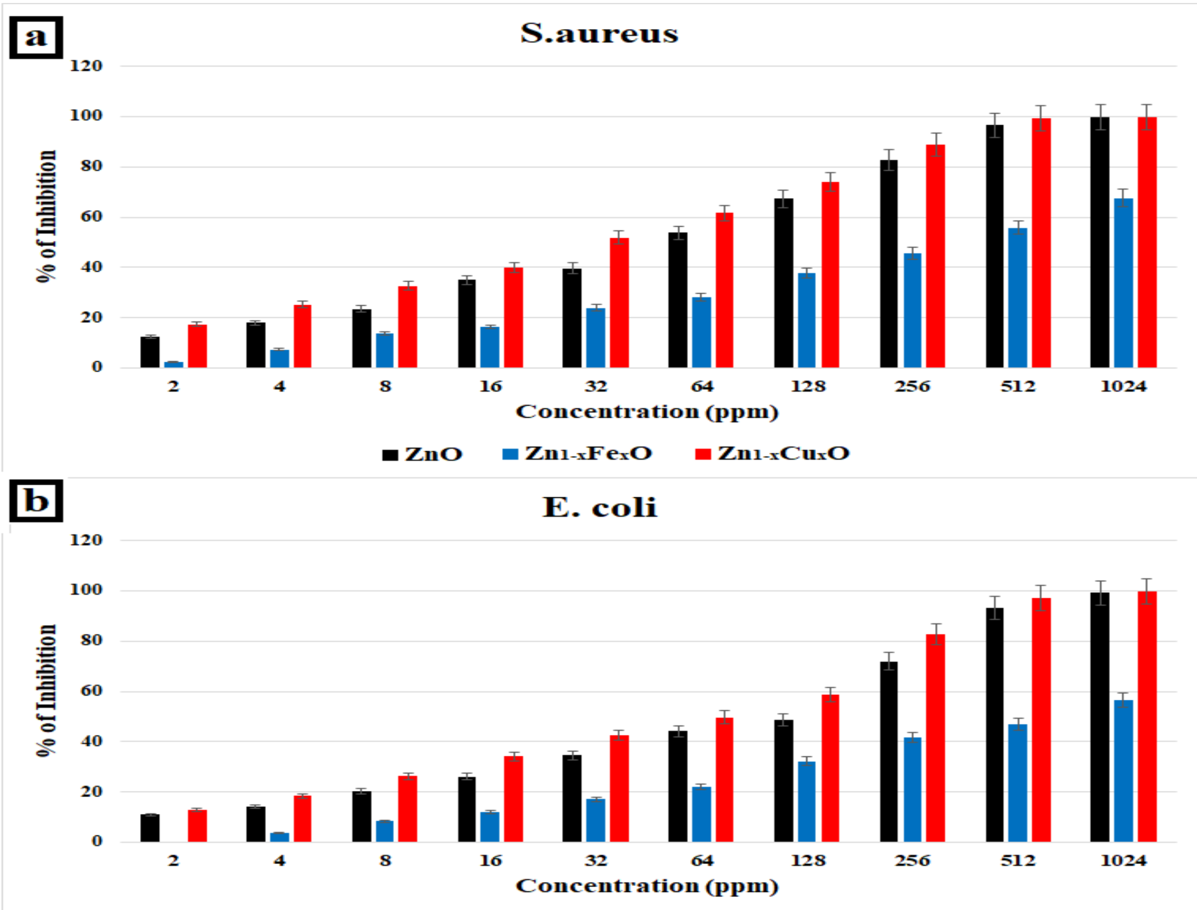

Fig. 7. Antibacterial effects of concentrations of 2 to 1024 ppm of NPs against (a) S. aureus and (b) E. coli bacteria

The 50% inhibitory concentration (IC-50) of the three synthesized NPs reported in Fig. 8, based on which the powerful substance used is $Zn_{1-x}Cu_xO$ NPs, whose IC-50 for S. aureus and E. coli bacteria was 80.77 and 176.44 ppm, respectively, and the weakest of them was $Zn_{1-x}Fe_xO$ NPs, whose IC-50 for S. aureus and E. coli bacteria was 555.31 and 715.57 ppm, respectively.

The difference in antibacterial activity between Gram-positive S. aureus and Gram-negative E. coli is primarily due to structural variations in their cell walls. Gram-negative bacteria possess an outer membrane rich in lipopolysaccharides, which serves as an extra protective barrier against the entry of NPs. This outer membrane limits the permeability of NPs and reduces their direct interaction with the bacterial cell. Additionally, the negative charge on the outer membrane's phospholipids can repel positively charged NPs, further hindering their ability to penetrate the cell. Even when NPs breach this barrier, the periplasmic space—a region between the outer membrane and the thin peptidoglycan layer—contains enzymes capable of neutralizing reactive oxygen species (ROS) produced by NPs, thereby providing additional resistance. In opposition, Gram-positive bacteria have a thicker peptidoglycan layer but lack the outer membrane of Gram-negative bacteria. This structural simplicity allows NPs to access the cell more easily. The interaction of positively charged copper ions with the negatively charged teichoic acids within the Gram-positive cell wall may also lead to more effective bacterial membrane disruption and enhanced ROS generation, contributing to their increased susceptibility. The structural and biochemical differences between Gram-positive and Gram-negative bacteria highlight the strong antibacterial effects of copper-doped NPs specifically against Gram-positive species, as indicated by previous studies [48, 49].

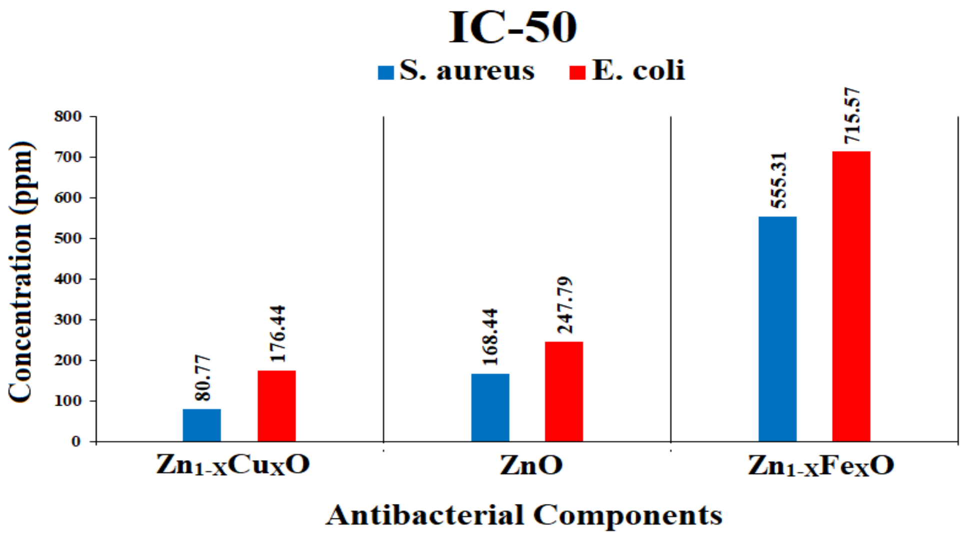

Fig. 8. The amount of IC-50 (Inhibitory Concentration 50%) related to NPs synthesized on S. aureus and E. coli bacteria

The results of Fig. 9a were analyzed by SPSS software. Fig. 9 shows that cell survival was alleviated by enhancing NP concentration. The percentage of cell death induced was determined using the MTT assay. The percentage of viable cells compared to the control illustrates that ZnO and $Zn_{1-x}Fe_xO$ at a concentration of 50 μg/ml did not have a lethal on cancer cells, but at other concentrations, they have a lethal on cancer cells. Comparing ZnO and $Zn_{1-x}Fe_xO$ with each other on cancer cells, the results show no significant difference in the lethal on cancer cells, while $Zn_{1-x}Cu_xO$ in all concentrations has a lethal on cancer cells more meaningful than ZnO and $Zn_{1-x}Fe_xO$ in various concentrations. Fig. 9b, after loading the drug on the NPs, shows that NPs have significantly increased the anticancer properties of the sunitinib drug in different concentrations. Two NPs of ZnO and $Zn_{1-x}Fe_xO$ acted almost similarly to each other, while $Zn_{1-x}Cu_xO$ has significantly increased the anticancer effect of the drug compared to the other NPs, sunitinib@$Zn_{1-x}Cu_xO$ destroyed 92% of cancer cells in 200 μg/ml concentration. Copper participates in redox reactions through Fenton-like processes, cycling between Cu(I) and Cu(II) states. This redox activity generates reactive oxygen species (ROS), such as hydroxyl radicals (*OH*) and superoxide ions (*O_2^{-}*), which can damage cellular macromolecules, including DNA, proteins, and lipids. Cancer cells, already under higher oxidative stress, are particularly susceptible to further ROS-induced damage. Zinc is redox-inactive and does not participate in similar ROS-generating reactions. While zinc ions can contribute to anticancer effects by stabilizing biomolecules and enzymes, its impact on oxidative stress is minimal compared to copper [50, 51]. Excess copper disrupts the delicate balance of intracellular metal ions. Copper overload interferes with the function of metalloproteins and enzymes, leading to cellular dysfunction and apoptosis. Copper targets mitochondria, leading to mitochondrial membrane potential collapse, ROS overproduction, and inhibition of oxidative phosphorylation. This can trigger apoptosis via mitochondrial pathways [50, 52]. Our results show that ZnO, $Zn_{1-x}Cu_xO$, and $Zn_{1-x}Fe_xO$ NPs demonstrated less cytotoxic effects on the cancer cell line at low concentrations. The anticancer result showed that the prepared NPs and the drug-loaded on them could be useful as targets against cancer cells.

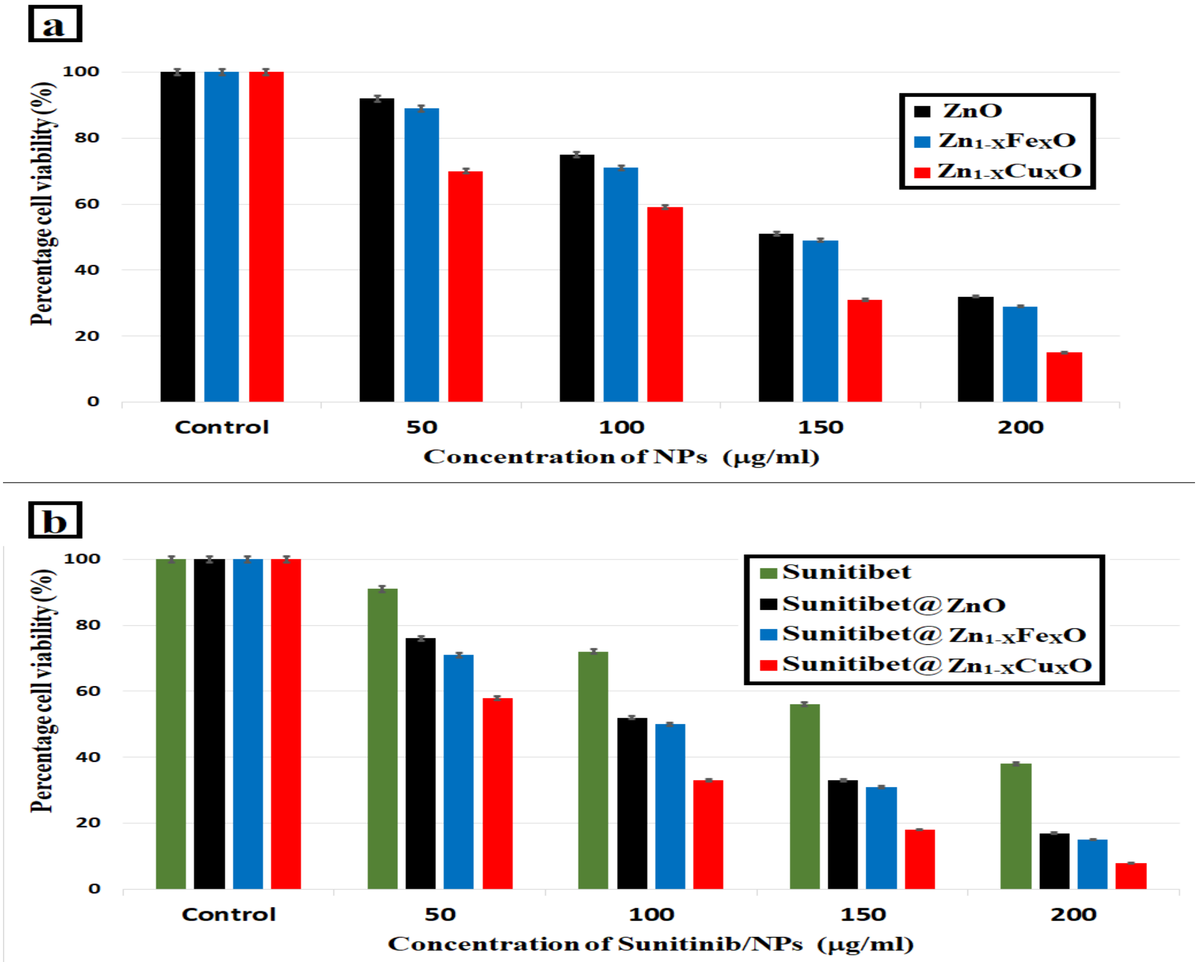

Fig. 9. Cytotoxic effect of (a) NPs and (b) Sunitinib@NPs in AsPC-1 cell lines at various concentrations (50, 100, 150, and 200 µg/mL) of NPs for 48h

5. Conclusion

This study has presented a low-cost and simple route with a short synthesis time for NPs using the sol-gel method. The structural characterizations confirmed the formation of the hexagonal wurtzite type ZnO nanostructure without extra peaks with different crystal sizes and morphologies. The antioxidant activity showed adding impurity improved the antioxidant properties, and copper dopant was more suitable than iron by 88.98. The inhibition percentage of S. aureus and E. coli bacteria by NPs was investigated, among the bacterial samples tested, S. aureus bacterium (gram-positive) was more sensitive to NPs, and E. coli (gram-negative) bacterium showed more resistance to NPs. The powerful substance used is $Zn_{1-x}Cu_xO$ NPs for S. aureus and E. coli bacteria at 80.77 and 176.44 ppm, respectively. Also, the weakest is $Zn_{1-x}Fe_xO$ NPs for S. aureus and E. coli bacteria at 555.31 and 715.57 ppm, respectively. The study explored the scavenging properties of DPPH free radicals, a well-known stable free radical frequently used in the assessment of antioxidant activity. Additionally, the anticancer effects of NPs were examined on the AsPC-1 cell line, which is derived from pancreatic cancer cells. The purpose of this research was to assess whether NPs have antioxidant properties and could restrain the proliferation of cancerous cells. The results obtained from assays showed that drugs loaded on NPs were better than drugs in the studies. Two NPs of ZnO and $Zn_{1-x}Fe_xO$ acted almost similar to each other. At the same time, $Zn_{1-x}Cu_xO$ has significantly increased the anticancer effect of the drug compared to the other NPs, so sunitinib@$Zn_{1-x}Cu_xO$ destroyed 92% of cancer cells in 200 µg/ml concentration.

References

[1] Are, C., et al., *Global Cancer Surgery: pragmatic solutions to improve cancer surgery outcomes worldwide.* The Lancet Oncology, 2023. 24(12): p. e472-e518.

[2] Mohamed, M., et al., *A scoping review evaluating physical and cognitive functional outcomes in cancer survivors treated with chemotherapy: charting progress since the 2018 NCI think tank on cancer and aging phenotypes.* Journal of Cancer Survivorship, 2024: p. 1-42.

[3] Wang, L., et al., *Radiotherapy and immunology.* Journal of Experimental Medicine, 2024. 221(7): p. e20232101.

[4] Cassinello, F., et al., *Cancer surgery: how may anesthesia influence outcome?* Journal of clinical anesthesia, 2015. 27(3): p. 262-272.

[5] Grigorian, A. and C.B. O'Brien, *Hepatotoxicity secondary to chemotherapy.* Journal of clinical and translational hepatology, 2014. 2(2): p. 95.

[6] Wang, S., et al., *Cancer treatment-induced accelerated aging in cancer survivors: biology and assessment.* Cancers, 2021. 13(3): p. 427.

[7] Faye, G., T. Jebessa, and T. Wubalem, *Biosynthesis, characterisation and antimicrobial activity of zinc oxide and nickel doped zinc oxide nanoparticles using Euphorbia abyssinica bark extract.* IET nanobiotechnology, 2022. 16(1): p. 25-32.

[8] Carofiglio, M., et al., Doped zinc oxide nanoparticles: synthesis, characterization and potential use in nanomedicine. Applied Sciences, 2020. 10(15): p. 5194.

[9] Mehrizi, T.Z. and K.M. Hosseini, *An overview on the investigation of nanomaterials' effect on plasma components: immunoglobulins and coagulation factor VIII, 2010–2020 review.* Nanoscale Advances, 2021. 3(13): p. 3730-3745.

[10] Hashmi, M.U., et al., *Hydrogels incorporated with silver nanocolloids prepared from antioxidant rich Aerva javanica as disruptive agents against burn wound infections.* Colloids and Surfaces A: Physicochemical and Engineering Aspects, 2017. 529: p. 475-486.

[11] Jiang, J., J. Pi, and J. Cai, *The advancing of zinc oxide nanoparticles for biomedical applications.* Bioinorganic chemistry and applications, 2018. 2018.

[12] Vindhya, P., et al., *Antimicrobial, antioxidant, cytotoxicity and photocatalytic performance of Co doped ZnO nanoparticles biosynthesized using Annona Muricata leaf extract.* Journal of Environmental Health Science and Engineering, 2023. 21(1): p. 167-185.

[13] Armelao, L., et al., *Photocatalytic and antibacterial activity of TiO2 and Au/TiO2 nanosystems.* Nanotechnology, 2007. 18(37): p. 375709.

[14] Shi, L.-E., et al., *Synthesis, antibacterial activity, antibacterial mechanism and food applications of ZnO nanoparticles: a review.* Food Additives & Contaminants: Part A, 2014. 31(2): p. 173-186.

[15] Sharma, S., et al., *Eco-friendly Ocimum tenuiflorum green route synthesis of CuO nanoparticles: Characterizations on photocatalytic and antibacterial activities.* Journal of Environmental Chemical Engineering, 2021. 9(4): p. 105395.

[16] Wang, S., et al., *Antibacterial activity of nano-SiO2 antibacterial agent grafted on wool surface.* Surface and Coatings Technology, 2007. 202(3): p. 460-465.

[17] Amininezhad, S.M., et al., *The antibacterial activity of SnO2 nanoparticles against Escherichia coli and Staphylococcus aureus.* Zahedan Journal of Research in Medical Sciences, 2015. 17(9).

[18] Abinaya, S. and H.P. Kavitha, *Magnesium oxide nanoparticles: effective antilarvicidal and antibacterial agents.* ACS omega, 2023. 8(6): p. 5225.

[19] Hariharan, D., et al., *Enhanced photocatalysis and anticancer activity of green hydrothermal synthesized Ag@ TiO2 nanoparticles.* Journal of Photochemistry and Photobiology B: Biology, 2020. 202: p. 111636.

[20] Gebreslassie, Y.T. and F.G. Gebremeskel, *Green and cost-effective biofabrication of copper oxide nanoparticles: Exploring antimicrobial and anticancer applications.* Biotechnology Reports, 2024: p. e00828.

[21] Albo Hay Allah, M.A. and H.A. Alshamsi, *Green synthesis of ZnO NPs using Pontederia crassipes leaf extract: characterization, their adsorption behavior and anti-cancer property.* Biomass Conversion and Biorefinery, 2024. 14(9): p. 10487-10500.

[22] Khan, M.R., et al., *Evaluation of biogenically synthesized MgO NPs anticancer activity against breast cancer cells.* Saudi Journal of Biological Sciences, 2024. 31(1): p. 103874.

[23] Moorer, W. and J. Genet, *Antibacterial activity of gutta-percha cones attributed to the zinc oxide component.* Oral Surgery, Oral Medicine, Oral Pathology, 1982. 53(5): p. 508-517.

[24] Florence, A. and G. Halbert, *Drug delivery and targeting.* Physics in Technology, 1985. 16(4): p. 164.

[25] Majeed, S., et al., *Anticancer and apoptotic activity of biologically synthesized zinc oxide nanoparticles against human colon cancer HCT-116 cell line-in vitro study.* Sustainable Chemistry and Pharmacy, 2019. 14: p. 100179.

[26] Shochah, Q.R. and F.A. Jabir, *Green synthesis of Au/ZnO nanoparticles for anticancer activity and oxidative stress against MCF-7 cell lines.* Biomass Conversion and Biorefinery, 2023: p. 1-14.

[27] Othman, M.S., et al., Antitumor activity of zinc nanoparticles synthesized with berberine on human epithelial colorectal adenocarcinoma (Caco-2) cells through acting on Cox-2/NF-kB and p53 pathways. Anti-Cancer Agents in Medicinal Chemistry (Formerly Current Medicinal Chemistry-Anti-Cancer Agents), 2022. 22(10): p. 2002-2010.

[28] Mongy, Y. and T. Shalaby, *Green synthesis of zinc oxide nanoparticles using Rhus coriaria extract and their anticancer activity against triple-negative breast cancer cells.* Scientific Reports, 2024. 14(1): p. 13470.

[29] Jain, A., R. Bhargava, and P. Poddar, *Probing interaction of Gram-positive and Gram-negative bacterial cells with ZnO nanorods.* Materials Science and Engineering: C, 2013. 33(3): p. 1247-1253.

[30] Slman, A.A., *Antibacterial activity of Zno nanoparticle on some gram-positive and gram-negative bacteria.* Iraqi Journal of physics, 2012. 10(18): p. 5-10.

[31] Dadi, R., et al., *Antibacterial activity of ZnO and CuO nanoparticles against gram positive and gram negative strains.* Materials Science and Engineering: C, 2019. 104: p. 109968.

[32] Li, Y., C. Liao, and S.C. Tjong, *Recent advances in zinc oxide nanostructures with antimicrobial activities.* International Journal of Molecular Sciences, 2020. 21(22): p. 8836.

[33] Morshed, M.N., et al., *Antioxidant activity of Panax ginseng to regulate ROS in various chronic diseases.* Applied Sciences, 2023. 13(5): p. 2893.

[34] Manouchehri, I., et al., *Investigation of annealing effects on optical properties of Ti thin films deposited by RF magnetron sputtering.* Optik, 2016. 127(13): p. 5383-5389.

[35] Miliauskas, G., P. Venskutonis, and T. Van Beek, *Screening of radical scavenging activity of some medicinal and aromatic plant extracts.* Food chemistry, 2004. 85(2): p. 231-237.

[36] Li, H.-y., et al., *Antioxidant activities of extracts and fractions from Lysimachia foenum-graecum Hance.* Bioresource technology, 2009. 100(2): p. 970-974.

[37] Fatahi Dehpahni, M., K. Chehri, and M. Azadbakht, *Effect of Silver nanoparticles and l-carnitine supplement on mixed*

vaginitis caused by Candida albicans/Staphylococcus aureus in Mouse Models: An Experimental Study. Current Microbiology, 2021. 78: p. 3945-3956.

[38] Dehpahni, M.F., K. Chehri, and M. Azadbakht, *Therapeutic effects of silver nanoparticle and L-carnitine on aerobic vaginitis in mice: an experimental study.* BioImpacts: BI, 2022. 12(1): p. 33.

[39] Niu, J., et al., *Identification and functional studies of microbial volatile organic compounds produced by Arctic flower yeasts.* Frontiers in Plant Science, 2023. 13: p. 941929.

[40] Al-Enazi, N.M., et al., *In vitro anticancer and antibacterial performance of biosynthesized Ag and Ce co-doped ZnO NPs.* Bioprocess and Biosystems Engineering, 2023. 46(1): p. 89-103.

[41] Santosa, S.J., S. Sudiono, and R.S. Wibawani, *Solvent-free mechanochemically synthesized Zn layered hydroxide salts for the adsorption of naphtholate AS dye.* Applied Surface Science, 2020. 506: p. 144930.

[42] Kiziltaş, H., T. Tekin, and D. Tekin, *Synthesis, characterization of Fe3O4@ SiO2@ ZnO composite with a core-shell structure and evaluation of its photocatalytic activity.* Journal of Environmental Chemical Engineering, 2020. 8(5): p. 104160.

[43] Sridhar, A., et al., *Dual doping effect of Ag+ & Al3+ on the structural, optical, photocatalytic properties of ZnO nanoparticles.* Applied Surface Science Advances, 2023. 13: p. 100382.

[44] Abhijith, A., A. Srivastava, and A. Srivastava. *Synthesis and characterization of magnesium doped ZnO using chemical route*. in *Journal of Physics: Conference Series*. 2020. IOP Publishing.

[45] Xiong, G., et al., *Photoluminesence and FTIR study of ZnO nanoparticles: the impurity and defect perspective.* physica status solidi c, 2006. 3(10): p. 3577-3581.

[46] Christodoulou, M.C., et al., *Spectrophotometric Methods for Measurement of Antioxidant Activity in Food and Pharmaceuticals.* Antioxidants, 2022. 11(11): p. 2213.

[47] Kedare, S.B. and R. Singh, *Genesis and development of DPPH method of antioxidant assay.* Journal of food science and technology, 2011. 48: p. 412-422.

[48] Lehman, K.M. and M. Grabowicz, *Countering gram-negative antibiotic resistance: Recent progress in disrupting the outer membrane with novel therapeutics.* Antibiotics, 2019. 8(4): p. 163.

[49] Ebbensgaard, A., et al., The role of outer membrane proteins and lipopolysaccharides for the sensitivity of Escherichia coli to antimicrobial peptides. Frontiers in microbiology, 2018. 9: p. 2153.

[50] Ji, P., et al., *Potential of copper and copper compounds for anticancer applications.* Pharmaceuticals, 2023. 16(2): p. 234.

[51] Tang, X., et al., *Copper in cancer: from limiting nutrient to therapeutic target.* Frontiers in Oncology, 2023. 13: p. 1209156.

[52] Vo, T.T.T., et al., *The crosstalk between copper-induced oxidative stress and cuproptosis: a novel potential anticancer paradigm.* Cell Communication and Signaling, 2024. 22(1): p. 353.